Journal of Solid State Chemistry 183 (2010) 600–605

Contents lists available at ScienceDirect

Journal of Solid State Chemistry

journal homepage: www.elsevier.com/locate/jssc

A Facile synthesis of flower-like Co_3O_4 porous spheres for the lithium-ion battery electrode

Jun Zheng, Jing Liu, Dongping Lv, Qin Kuang, Zhiyuan Jiang *, Zhaoxiong Xie, Rongbin Huang, Lansun Zheng

State Key Laboratory for Physical Chemistry of Solid Surfaces and Department of Chemistry, College of Chemistry and Chemical Engineering, Xiamen University, Xiamen 361005, PR China

ARTICLE INFO

Article history:
Received 11 September 2009
Received in revised form
24 November 2009
Accepted 19 December 2009
Available online 4 January 2010

Keywords:
Co_3O_4
Porous structures
Nanostructures
Lithium-ion battery

ABSTRACT

The porous hierarchical spherical Co_3O_4 assembled by nanosheets have been successfully fabricated. The porosity and the particle size of the product can be controlled by simply altering calcination temperature. SEM, TEM and SAED were performed to confirm that mesoporous Co_3O_4 nanostructures are built-up by numerous nanoparticles with random attachment. The BET specific surface area and pore size of the product calcined at 280 °C are 72.5 $m^2 g^{-1}$ and 4.6 nm, respectively. Our experiments further demonstrated that electrochemical performances of the synthesized products working as an anode material of lithium-ion battery are strongly dependent on the porosity.

1. Introduction

Rechargeable lithium-ion batteries have been the most utilized batteries in portable electronic equipment because of the high energy density and good safety. A large number of studies have demonstrated that transition metal oxides are promising anode materials of rechargeable lithium-ion batteries [1,2]. However, transition metal oxides have been hampered by poor capacity retention upon cycling, which remain major challenges in practical application. To use porous nanomaterials of transition metal oxides as the anode of lithium-ion batteries is one possible strategy to alleviate the problem. The main reason is that these porous nanomaterials own high electrode–electrolyte contact area, short path length for Li^+ transport, and good strain accommodation, compared with other solid nanostructures [3–8].

As one of the promising potential electrode materials for lithium-ion batteries, Co_3O_4 with high theoretical capacity has received considerable attention over the last few years [3–14]. Up to now, several Co_3O_4 nanostructures such as nanoparticles, nanorods, nanocubes, nanowires, flowers, hollow spheres, nanoboxes and porous structure have been synthesized by means of various routes [15–26]. However, it is still a challenging research area to explore simple methods for the synthesis of mesoporous architectures of Co_3O_4 with high specific surface area and large pore volume for the application in rechargeable lithium-ion batteries.

Herein, we report a simple calcination process to prepare flower-like porous spherical Co_3O_4 from α-phases cobalt hydroxide precursor. These flower-like Co_3O_4 porous spheres have a hierarchical structure with high specific surface area and large pore volume. Moreover, the porosity and particle size of the product architecture can be altered by controlling the calcination temperature. When flower-like Co_3O_4 porous spheres was evaluated on Co_3O_4/Li coin cell, the Co_3O_4 had the high discharge capacity of 1316.7 mAh g^{-1} in the first cycle and retain lithium storage capacity of about 600 mAh g^{-1} after 10 cycles. The electrochemical experiments demonstrated that the porosity and smaller particle size will help to improve the electrochemical properties.

2. Experimental details

2.1. Synthesis of the sample

All the reagents used in the experiments were of analytical grade, and used as received without further purification. Cobalt nitrate hexahydrate ($Co(NO_3)_2 \cdot 6H_2O$) and sodium hydroxide (NaOH) purchased from Sinopharm Chemical Reagent Co., Ltd. Succinic acid ($(CH_2COOH)_2$) is purchased from Shantou Xilong Chemical Factory (Guangdong, China). The synthesis of flower-like Co_3O_4 porous nanostructures involves two steps: formation of the flower-like precursor α-$Co(OH)_2$ at solvothermal conditions and sequent calcination to Co_3O_4 at higher temperature. In a

* Corresponding author. Fax: +86 592 2183047.
E-mail address: zyjiang@xmu.edu.cn (Z. Jiang).

0022-4596/$ - see front matter © 2009 Elsevier Inc. All rights reserved.
doi:10.1016/j.jssc.2009.12.017

typical synthesis, 0.04 g of NaOH and 0.024 g of $(CH_2COOH)_2$ were added into 2 mL of deionized water and 8 mL of ethanol and stirred until totally dissolved. The pH value of the solution was adjusted to approximately 3, and 0.291 g of $Co(NO_3)_2 \cdot 6H_2O$ was added. The resulting solution was transferred into a Teflon-lined stainless autoclave with a capacity of 22 ml, kept at 150 °C for 2 h, and then quickly cooled to ambient temperature. The precursor product was collected by centrifugation and washed with absolute ethanol several times. The final product, flower-like Co_3O_4 porous nanostructure was obtained by the calcination of the precursor at different temperatures (typically 280 °C) for 1 h.

2.2. Characterizations of the sample

The composition and phase of the precursor and the final products were determined by X-ray diffraction (XRD, PANalytical X-Pert diffractometer with Cu-*K*α radiation). The morphology and structure of the final products were obtained by field emission scanning electron microscopy (SEM, LEO1530) and high resolution transmission electron microscopy (HRTEM, JEM-2100 and FEI Tecnai-F30 FEG). Thermogravimetry (TG) analysis was carried out on SDT Q600 thermal analyzer under an air atmosphere at the temperature range of 30–500 °C with a heating rate of 5 °C min^{-1}. The surface area of the final products was measured by the Brunauer–Emmett–Teller (BET) method using nitrogen adsorption and desorption isotherms on a Micrometrics ASAP 2020 system. Pore size distribution plot was obtained by Barrett–Joyner–Halenda (BJH) method.

2.3. Electrochemical measurement of the sample

The electrochemical properties of the as-prepared flower-like Co_3O_4 porous nanostructures were carried out using coin cells with lithium metal as the counter electrodes. The 80 wt% Co_3O_4 was mixed with 10 wt% acetylene black and 10% polyvinylidene fluoride. The mixture was pressed onto copper (current collector) and thereafter dried at 110 °C under vacuum for 2 h to obtain the working electrode. Coin cells were assembled with the prepared working electrode, lithium and separator (Celgard 2400 polypropylene) in a glove-box filled with pure argon. The electrolyte was 1 M $LiPF_6$ in ethylene carbonate/dimethyl carbonate (1:1 V/V). The cells were cycled at a constant temperature of 30 °C. For cycling experiments, the cells were charged and discharged in a potential range of 0.01 and 3 V at various current densities of 50 and 300 mA g^{-1}, respectively.

3. Results and discussion

The general morphology of the as-prepared flower-like precursor synthesized via the solvothermal route is shown in Fig. 1. It is clearly seen from the low-magnification image (Fig. 1a) that most particles in the precursor are of a spherical structure with a size of 3–4 μm. A closer observation (Fig. 1b) displays that these spheres are hierarchical and composed of large numbers of nanosheets with smooth surfaces. The observed nanosheets are 400–500 nm in size and 30–40 nm in thickness, are connected with each other at the root to build flower-like hierarchical spheres. It is noteworthy that without the existence succinic acid, no such flower-like hierarchical spheres were observed in the products. It is reported that succinic acid can coordinate with Co^{2+} to form complex [27], which may control the hydrolysis rate and thus significantly influences the morphology of the products. In addition, $Co(OH)_2$ is easy to be directly precipitated in an alkalescent solution, which may lead to uncontrollability of the morphology. As a result, the pH of the solution should be adjusted to about 3 before the hydrothermal process, by which $Co(OH)_2$ with a morphology of hierarchical spheres can be formed via a slow hydrolysis of Co^{2+}.

The composition and phase of the hierarchical flower-like precursor were determined by further XRD and TG analysis. As shown in Fig. 2a, the XRD pattern (the bottom line) of the precursor consists of three prominent diffraction peaks at 10°(d1), 20°(d2) and 34°(d3), the d spacing of which is 8.71, 4.34, and 2.62 Å, respectively. This pattern can be indexed to α-phase of cobalt hydroxide although the d spacing of the precursor is slight variation due to the intercalation of some anion species [28–33]. However, α-phase of cobalt hydroxide is not well-crystallized suggested by the peak intensity. Fig. 2b shows the TG curve of the precursor, clearly displaying a two step weight loss due to dehydration and decomposition of the α-phase of cobalt hydroxide, respectively. The weight loss of 10% at the low temperature (50–165 °C) is related to adsorbed and intercalated water of α-cobalt hydroxide, while the weight loss of 25% from 165 to 255 °C corresponds to the loss of structural water and thermal oxidative decomposition [28–30].

The composition and phase of the products after thermal decomposition are confirmed by corresponding XRD patterns. As shown in Fig. 2a, the curves labeled as sample 1 and sample 2 correspond to the products at the calcining temperatures of 280 and 500 °C, respectively. It is clearly seen that all diffraction peaks of the samples 1 and 2 agree well with the cubic structure of pure Co_3O_4 (JCPDS 43-1003). No peaks from other phases have been detected, indicating a total decomposition of the precursor after the calcination. Nevertheless, the diffraction peaks of the sample 1 calcined at 280 °C exhibit a significant widening, in comparison

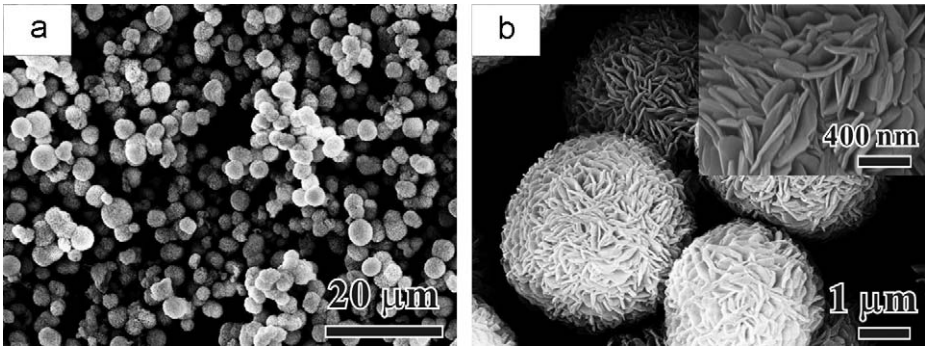

Fig. 1. (a) Low magnification and (b) high magnification SEM images of the precursor synthesize at 150 °C for 2 h via the solvothermal route. The inset is a partial enlarged SEM image.

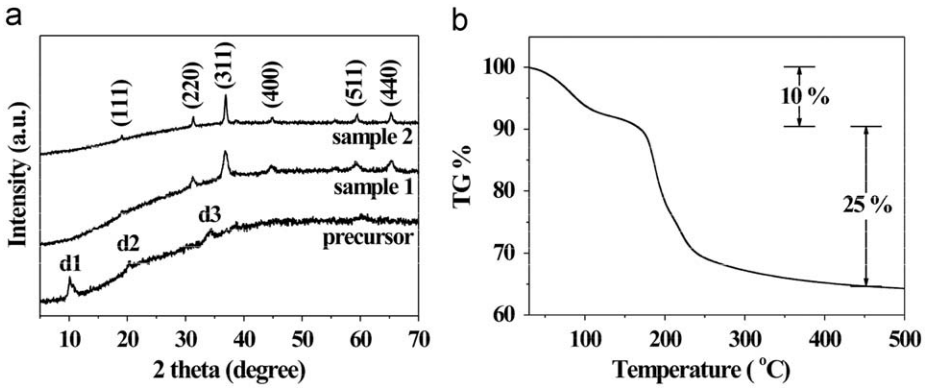

Fig. 2. (a) XRD patterns of the precursor and Co_3O_4 and (b) TG curve for the as-synthesized precursor respectively.

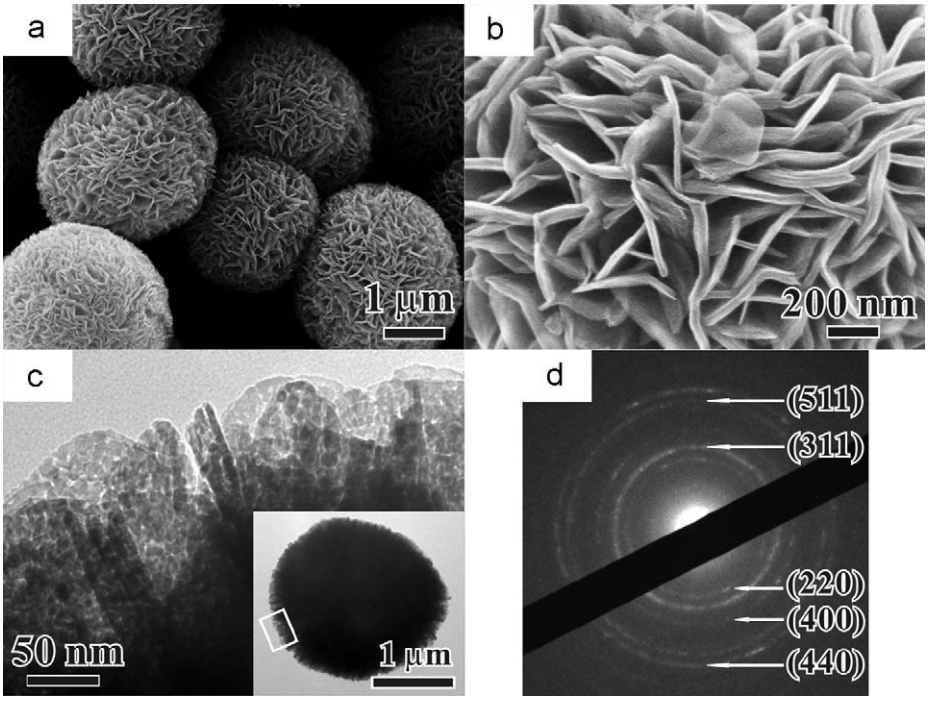

Fig. 3. (a) Low magnification and (b) high magnification SEM images of the sample 1 obtained at 280 °C, (c) detailed high magnification TEM image taken from the edge of the as prepared Co_3O_4 sphere (inset) and (d) the corresponding SAED pattern of an individual flower-like Co_3O_4 hierarchical sphere in the sample 1.

with the sample 2. According to the Scherrer equation, the mean size of the crystallite in the sample 1 is calculated to be only about 13 nm while the calculated value of the sample 2 is up to 33 nm. These results indicate that the products after the calcination are consisted of numerous Co_3O_4 nanocrystallites, and at the same time the nanocrystallite size increases with the calcining temperature.

Fig. 3a displays a typical SEM image of the sample 1 obtained by calcination of the flower-like precursor at 280 °C, clearly showing that the calcined Co_3O_4 product still retains overall morphology of the flower-like precursor. It can be seen from corresponding high-magnification SEM image (Fig. 3b) that the nanosheets forms flower-like hierarchical spheres, which are still about 35 nm in the thickness and 400–500 nm the size, did not present obvious morphological deformation in comparison with the precursor. More detailed structural information was provided by TEM observation. Fig. 3c is a typical HRTEM image taken from the edge of an individual hierarchical sphere shown in the inset. From this Figure, it can be seen that each nanosheet of the flower-like hierarchical spheres has became a highly porous structure consisting of interconnected nanoparticles. The size of these nanoparticles ranged between 10 and 15 nm, consistent with the XRD result calculated from the Scherrer equation. The corresponding selected-area electron diffraction (SAED) pattern (Fig. 3d) further confirms that the as-obtained flower-like Co_3O_4 hierarchical structure is polycrystalline in nature, and the connection between the nanoparticles is disordered, not following the orientated attachment. After calcination, each nanosheet of the flowerlike structure had been transformed from nanosheet with a smooth surface into porous structure consisting of interconnected nanoparticles, because of releasing water vapor in the precursor during the calcination process [34].

Calcination temperature is the key factor for controlling porous structure and particle sizes of as-prepared Co_3O_4 spheres. Fig. 4a displays SEM image of the Co_3O_4 (sample 2) calcined at 500 °C. From its high magnification SEM image (Fig. 4b), the nature of the sphere is built up by primary nanosheets and the nanosheets-shaped obviously consist of large numbers of nanoparticles with the size about 35 nm, which is well consistent with the XRD result. The SAED pattern of Co_3O_4 sphere also suggests that the

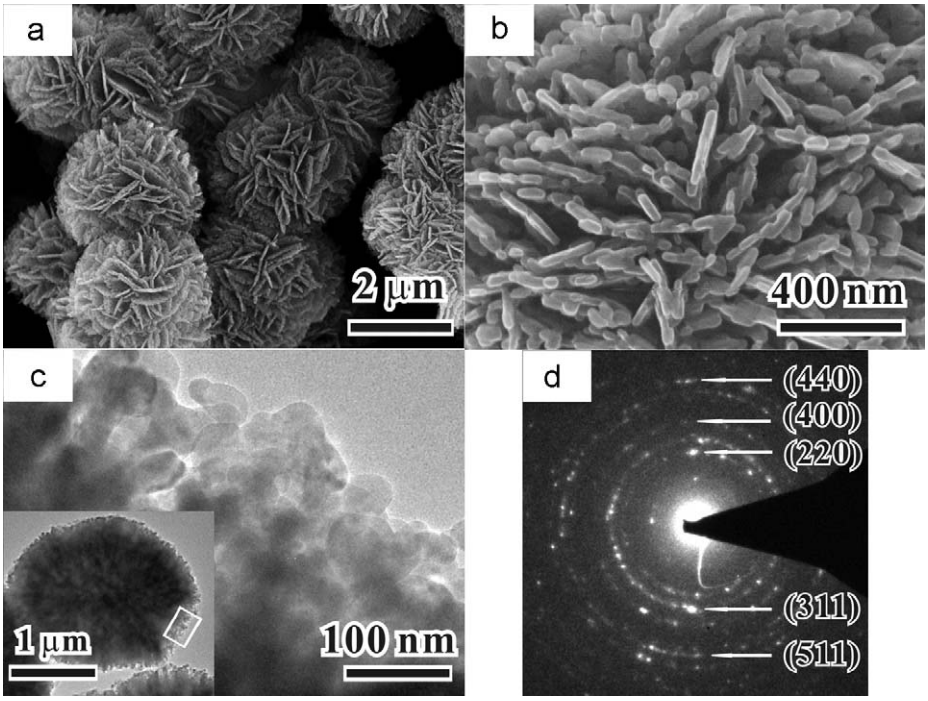

Fig. 4. (a) Low magnification and (b) high magnification SEM images of the sample 2 obtained at 500 °C, (c) detailed high magnification TEM image taken from the edge of an individual flower-like Co_3O_4 hierarchical sphere (inset) in the sample 2 and (d) the corresponding SAED pattern of the sphere.

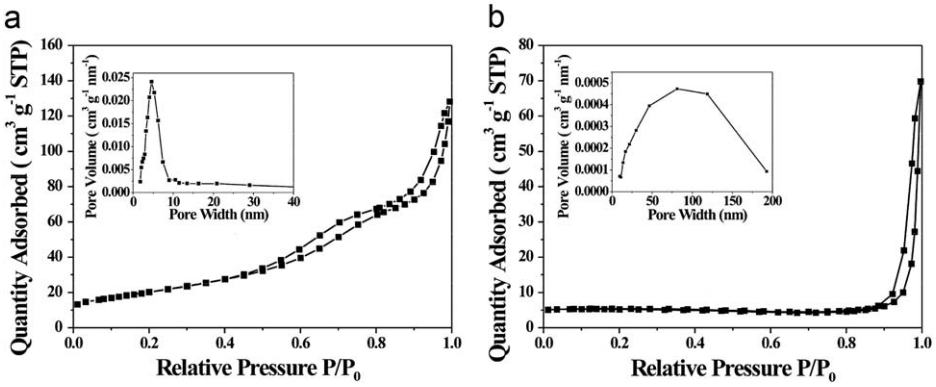

Fig. 5. Nitrogen adsorption–desorption isotherm measured by ASAP 2020 for mesoporosity and BJH pore size distribution plot (inset): (a) sample 1 and (b) sample 2.

nanoparticles in the sample 2 are randomly attached together (Fig. 4c–d). When the calcination temperature was elevated 700 °C, the size of the primary nanoparticles was increased to about 100 nm. It is interesting that the morphology of flower-like hierarchical spheres almost keep the same though the size of the primary nanoparticles becomes bigger with the elevated calcination temperature. With a suitable heating rate which may avoid the bursting out of water vapor, the removal of water does not damage the regular arrangement of Co, O atoms, and the nanocontact between each nanoparticle may stabilize the structure mechanically against fracture during the calcinations [35,36]. However, with high calcinations temperature, the small nanoparticles may grow up via complicated attaching and ripening.

Fig. 5 shows the N_2 adsorption–desorption isotherm of the samples. The Brunauer–Emmett–Teller (BET) specific surface area of the sample 1 is 72.5 $m^2 g^{-1}$ calculated from N_2 isotherms at 77 K. In addition, the pore size distribution diagram (the inset of Fig. 5a) based on Barrett–Joyner–Halenda (BJH) method clearly indicates that pore is in the mesoporous region, and the pore size distribution is very narrow, at around 4.6 nm. These results show that sample 1 has a relatively large specific surface area which is mainly due to the existence of mesopores embedded in the hierarchical spheres. However, the surface area of the products gradually decreased with the increase of the calcination temperature. For example, the BET surface area of the sample 2 sharply decreased to 17.3 $m^2 g^{-1}$, which indicates that the nanoparticles building the nanosheets become markedly large in size so that the mesopores between the nanoparticles disappeared when increasing the calcination temperature.

The preliminary electrochemical properties of the as-obtained flower-like Co_3O_4 hierarchical spheres have been investigated, inspired by this idea. The electrochemical performance of Co_3O_4 calcined at various temperatures, i.e. samples 1 and 2, were evaluated on Co_3O_4/Li coin cell. The first discharge curves of samples 1 and 2 at a low current density of 50 mA g^{-1} are shown in Fig. 6a. A higher discharge capacity of 1316.7 mAh g^{-1} was obtained for the sample 1 in the first discharge process, while a lower capacity of 1121.3 mAh g^{-1} for the sample 2. From the fully

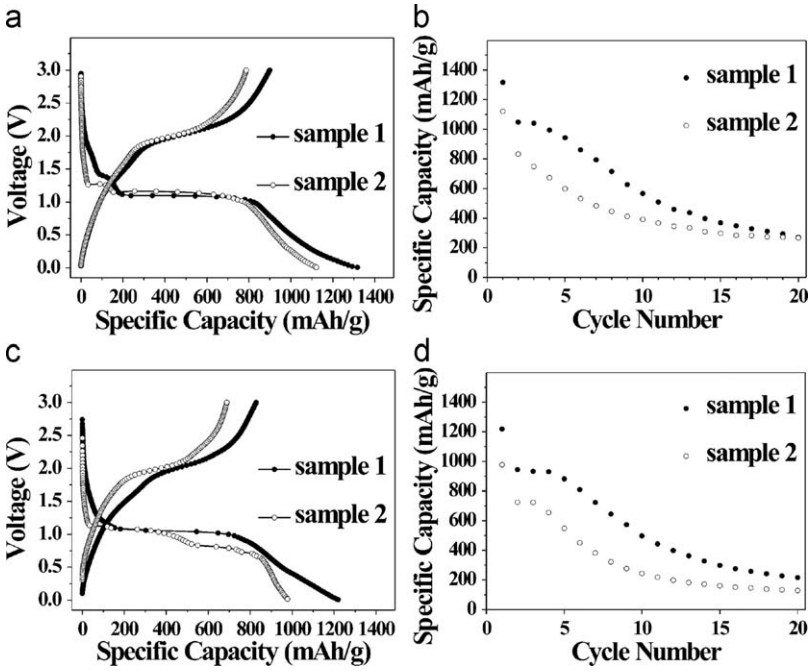

Fig. 6. (a and b) The first discharge–charge curves and cycling behavior of the sample 1 and sample 2 at a current density of 50 mA g^{-1} respectively; (c and d) The first discharge–charge curves and cycling behavior of the sample 1 and sample 2 at current density of 300 mA g^{-1}, respectively.

discharged state, 68.3%(899.1 mAh g^{-1}, sample 1) and 70.2% (787 mAh g^{-1}, sample 2) of the stored lithium can be extracted upon charging to 3 V, respectively. The reason for the existence of the initial irreversible capacity for anode materials is the formation of a solid electrolyte interface film, which forms on the surface of the anode material during the first discharge [37,38]. The cycling performances of samples 1 and 2 at a current density of 50 mA g^{-1} are presented in Fig. 6b. The discharge capacity of the sample 1 is higher than that of the sample 2 for each cycle. During the second discharge process, a discharge capacity of 1048 mAh g^{-1} and capacity retention of 79.6% were observed to sample 1, while the discharge capacity and capacity retention of sample 2 is 832.6 mAh g^{-1} and 74.3%, respectively.

As rate capability is an important parameter for applications of batteries, we also investigated the electrochemical performance of the samples at higher current density of 300 mA g^{-1}. As shown in Fig. 6c, good rate capability was observed on samples 1 and 2. For example, high discharge capacity of 1219.3 and 977.5 mAh g^{-1} were obtained in the first discharge process on samples 1 and 2, respectively. Such high capacities performed at high current rate are relatively rare to be reported [4,11]. From the cycling performance of the samples 1 and 2 at different current density (Fig. 6b,d), it can be concluded that sample 1 has a better electrochemical performances due to its higher specific surface area. The results are evidently believed to benefit from the unique structural features of porosity and smaller particle size of sample 1, because the porosity and smaller particle size will help to increase the electrolyte/Co_3O_4 contact area and shorten path length for Li^+ transport during the electrochemical reaction.

It should be pointed out that compared with the reported data of other Co_3O_4 nanostructures [3,4,10], the first discharge capacity of the sample 1 behaved pretty good but the cycling performance was comparatively low. As shown in Fig. 6b, the discharge capacity of the sample 1 gradually decreased during the first 5 cycles, and henceforth rapidly decayed. The storage capacity of the sample 1 retained about 600 mAh g^{-1} after 10 cycles but it was only 300 mAh g^{-1} after 20 cycles, close to that of sample 2. The deterioration of discharge capacity of sample 1 may be caused by the collapse of the unique mesoporous structure during the electrochemical reaction. Therefore, to improve the stability of the mesoporous structure may be a promising way to further improve their electrochemical properties.

4. Conclusion

Flower-like porous Co_3O_4 spheres assembled by nanosheets have been successfully fabricated by a simple calcination process from α-phases cobalt hydroxide precursors. SEM, TEM and SAED characterization confirmed that the nanosheets in mesoporous Co_3O_4 nanostructures are built-up by numerous nanoparticles with random attachment. The BET specific surface area and pore size of the product calcined at 280 °C are 72.5 m^2 g^{-1} and 4.6 nm, respectively. Importantly, the high initial discharge capacity of 1316.7 mAh g^{-1} was obtained for flower-like Co_3O_4 porous spheres due to its high surface area and unique mesoporous structure. In view of their porosity and simplicity in synthesis, the as-prepared Co_3O_4 nanostructures will be of interest for lithium-ion batteries, sensors, catalysts and other applications.

Acknowledgments

This work was supported by the National Natural Science Foundation of China (Grant nos. 20671078, 20725310, 20721001 and 20801045), the National Basic Research Program of China (Grant nos. 2007CB815303, 2009CB939804) and NCET in Fujian Province University.

References

[1] J.M. Tarascon, M. Armand, Nature 414 (2001) 359.
[2] P. Poizot, S. Laruelle, S. Grugeon, L. Dupont, J.M. Tarascon, Nature 407 (2000) 496.

[3] W.Y. Li, L.N. Xu, J. Chen, Adv. Funct. Mater. 15 (2005) 851.
[4] X.W. Lou, D. Deng, J.Y. Lee, L.A. Archer, J. Mater. Chem. 18 (2008) 4397.
[5] N. Du, H. Zhang, B.D. Chen, J.B. Wu, X.Y. Ma, Z.H. Liu, Y.Q. Zhang, D.R. Yang, X.H. Huang, J.P. Tu, Adv. Mater. 19 (2007) 4505.
[6] H. Zhang, J.B. Wu, C.X. Zhai, X.Y. Ma, N. Du, J.P. Tu, D.R. Yang, Nanotechnology 19 (2008) 035711.
[7] F.M. Zhan, B.Y. Geng, Y.J. Guo, Chem. Eur. J. 15 (2009) 6169.
[8] Y.G. Li, B. Tan, Y.Y. Wu, Nano Lett. 8 (2008) 265.
[9] K.T. Nam, D.W. Kim, P.J. Yoo, C.Y. Chiang, N. Meethong, P.T. Hammond, Y.M. Chiang, A.M. Belcher, Science 312 (2006) 885.
[10] Y. Liu, C.H. Mi, L.H. Su, X.G. Zhang, Electrochim. Acta 53 (2008) 2507.
[11] X.W. Lou, D. Deng, J.Y. Lee, J. Feng, L.A. Archer, Adv. Mater. 20 (2008) 258.
[12] X.H. Liu, G.Z. Qiu, X.G. Li, Nanotechnology 16 (2005) 3035.
[13] F.F. Tao, C.L. Gao, Z.H. Wen, Q. Wang, J.H. Li, Z. Xu, J. Solid State Chem. 182 (2009) 1055.
[14] H.C. Liu, S.K. Yen, J. Power Sources 166 (2007) 478.
[15] L. Fu, Z.M. Liu, Y.Q. Liu, B.X. Han, P.G. Hu, L.C. Cao, D.B. Zhu, Adv. Mater. 17 (2005) 217.
[16] E. Hosono, S. Fujihara, I. Honma, H.S. Zhou, J. Mater. Chem. 15 (2005) 1938.
[17] J. Feng, H.C. Zeng, Chem. Mater. 15 (2003) 2829.
[18] Y.G. Li, B. Tan, Y.Y. Wu, J. Am. Chem. Soc. 128 (2006) 14258.
[19] C. Nethravathi, S. Sen, N. Ravishankar, M. Rajamathi, C. Pietzonka, B. Harbrecht, J. Phys. Chem. B 109 (2005) 11468.
[20] L.X. Yang, Y.J. Zhu, L. Li, L. Zhang, H. Tong, W.W. Wang, G.F. Cheng, J.F. Zhu, Eur. J. Inorg. Chem. (2006) 4787.
[21] B.X. Li, Y. Xie, C.Z. Wu, Z.Q. Li, J. Zhang, Mater. Chem. Phys. 99 (2006) 479.
[22] A.M. Cao, J.S. Hu, H.P. Liang, W.G. Song, L.J. Wan, X.L. He, X.G. Gao, S.H. Xia, J. Phys. Chem. B 110 (2006) 15858.
[23] Y.S. Ding, L.P. Xu, C.H. Chen, X.F. Shen, S.L. Suib, J. Phys. Chem. C 112 (2008) 8177.
[24] T. He, D.R. Chen, X.L. Jiao, Y.Y. Xu, Y.X. Gu, Langmuir 20 (2004) 8404.
[25] T. He, D.R. Chen, X.L. Jiao, Y.L. Wang, Adv. Mater. 18 (2006) 1078.
[26] A. Rumplecker, F. Kleitz, E.L. Salabas, F. Schüth, Chem. Mater. 19 (2007) 485.
[27] P.M. Forster, N. Stock, A.K. Cheetham, Angew. Chem., Int. Ed. 44 (2005) 7608.
[28] M. Rajamathi, P.V. Kamath, R. Seshadri, Mater. Res. Bull. 35 (2000) 271.
[29] R.S. Jayashree, P.V. Kamath, J. Mater. Chem. 9 (1999) 961.
[30] J. Ismail, M.F. Ahmed, P.V. Kamath, G.N. Subbanna, S. Uma, J. Gopalakrishnan, J. Solid State Chem. 114 (1995) 550.
[31] V. Gupta, T. Kusahara, H. Toyama, S. Gupta, N. Miura, Electrochem. Commun. 9 (2007) 2315.
[32] P. Jeevanandam, Y. Koltypin, A. Gedanken, Y. Mastai, J. Mater. Chem. 10 (2000) 511.
[33] Z.G. Zhao, F.X. Geng, J.B. Bai, H.M. Cheng, J. Phys. Chem. C 111 (2007) 3848.
[34] L.S. Zhong, J.S. Hu, H.P. Liang, A.M. Cao, W.G. Song, L.J. Wan, Adv. Mater. 18 (2006) 2426.
[35] Z. Gui, R. Fan, W.Q. Mo, X.H. Chen, L. Yang, S.Y. Zhang, Y. Hu, Z. Z Wang, W.C. Fan, Chem. Mater. 14 (2002) 5053.
[36] C.C. Yu, L.X. Zhang, J.L. Shi, J.J. Zhao, J.H. Gao, D.S. Yan, Adv. Funct. Mater. 18 (2008) 1544.
[37] F. Orsini, A. Du Pasquier, B. Beaudoin, J.M. Tarascon, M. Trentin, N. Langenhuizen, E. De Beer, P. Notten, J. Power Sources 76 (1998) 19.
[38] S.L. Chou, J.Z. Wang, H.K. Liu, S.X. Dou, J. Power Sources 182 (2008) 359.